Dalton Transactions

Accepted Manuscript

ROYAL SOCIETY OF CHEMISTRY

www.rsc.org/dalton

Synthesis and characterization of ZnO/mpg-C_3N_4 heterojunction photocatalyst with enhanced visible light photoactivity

Daimei Chen*[1]*†, *Kewei Wang* [1,2,3]†, *Tiezhen Ren*[3], *Hao Ding*[1], *Yongfa Zhu*[2]

([1]National Laboratory of Mineral Materials, School of Materials Sciences and Technology, China University of Geosciences, Beijing 100083, China

[2]Department of Chemistry, Tsinghua University, Beijing, 100084, PR China

[3]School of Chemical Engineering, Hebei University of Technology, Tianjin 300130, China)

*Corresponding author.

Tel.: +86 10 82332274; fax: +86 10 82322974.

[1] E-mail: chendaimei@cugb.edu.cn; chendaimei0611.student@sina.com

[2] E-mail: zhuyf@tsinghua.edu.cn

Author Contributions

†These authors contributed equally to this work.

Abstract.

The ZnO/mpg-C_3N_4 composite photocatalyst with high visible light activity was successfully synthesized by a facile solvothermal method and characterized by thermogravimetric analysis (TGA), X-ray diffraction (XRD), transmission electron microscopy (TEM), high-resolution transmission electron microscopy (HRTEM) and UV-vis diffuse reflectance spectra (DRS). The results indicated that ZnO particles dispersed uniformly on the mpg-C_3N_4 sheet. The photocatalytic activity of ZnO/mpg-C_3N_4 for photodegradation of MB was much higher than that of pure mpg-C_3N_4 both under the visible light and simulated solar irradiation. The optimal ZnO content for the photocatalytic activity of the ZnO/mpg-C_3N_4 composites is 24.9%, which is almost 2.3 times as high as that of pure mpg-C_3N_4 under the visible light, and 1.9 times under the simulated solar irradiation. The enhancement in photocatalytic activity should be assigned to the effective separation and transfer of photogenerated charges coming from the well-matched overlapping band-structure between mpg-C_3N_4 and ZnO. Radical trap experiments show that both ZnO/mpg-C_3N_4 composites and mpg-C_3N_4 have the same photodegradation mechanism, and the holes are their main oxidative species for MB degradation.

Keyword: photocatalysis, mpg-C_3N_4, ZnO, solvothermal method

1. Introduction

Recently, removal of environmental pollutants through photocatalytic reaction has drawn increasing attention[1] because solar energy is an inexhaustible, low-cost, environmentally friendly energy resource. Photocatalysis is a catalytic process occurring on the surface of semiconductor materials under the irradiation of photons[2-6]. In the past decades, various semiconductor materials such as metal oxides[7], sulfides[8], nitrides[9], and their mixed solid solutions[10] have been exploited as photocatalysts for photocatalytic degradation of organic pollutants. Among them, ZnO shows high efficiency for photodegradation of some dyes in polluted water[11,12]. Unfortunately, very poor response to visible light and its high recombination rate of photogenerated charges limit its practical applications on a large scale. Accordingly, some effort has been devoted to reducing the recombination of photogenerated electron–hole pairs and improving the utilization of solar light of ZnO.

Since Wang et al. first reported that a polymeric semiconductor, graphite-like carbon nitride (g-C_3N_4), which was introduced as a metal-free photocatalyst for solar-driven applications[13]. This organic semiconductor offers new opportunities for photocatalysis due to its cheap availability, high stability, and especially its intrinsic visible light response[14,15]. However, the high recombination rate of photogenerated electron-hole pairs and low quantum efficiency limited the photocatalytic efficiency of pure g-C_3N_4. To enhance its photocatalytic capability, a number of methods have been exploited, including porous structures[16,27], doping with metal or nonmetal elements[18,19], coupling with grapheme[20,21], organic dyes[22] and other

semiconductors[23,24], texture engineering and molecular design[25,26], fabrication of CN/CNS heterojuncitons[27], modification of co-catalysts[25].

Coupling ZnO with g-C_3N_4 is may be an ideal system to improve the separation efficiency of photogenerated electron-hole pairs due to their well-matched overlapping band-structure. Qiu et al synthesized the g-C_3N_4–ZnO composite photocatalyst by a simple calcination process and its application for the photodegradation of Methyl Orange and p-nitrophenol experiments[28]. Wang et al synthesized the g-C_3N_4–ZnO composites with different weight percents of ZnO by a facile ball milling method or a heat treatment of the precursor.[29,30] The g-C_3N_4-ZnO composite exhibited the much higher photocatalytic activity than the single-phase g-C_3N_4, clearly demonstrating a synergistic effect between ZnO and g-C_3N_4. Our group has developed a ZnO photocatalyst hybridized with g-C_3N_4 and found that the introduction of g-C_3N_4 to ZnO not only can enhance the photocatalytic activity, but also successfully suppress the photocorrosion of ZnO[31,32].

Therefore, in this work, a facile solvothermal method was reported to synthesis a serial of ZnO/mpg-C_3N_4 composite photocatalysts. Mesoporous g-C_3N_4 (mpg-C_3N_4) with an open crystalline pore wall and a large surface area was used as a supporter to immobilize ZnO nanoparticles. The structure can in principle enhance the light harvesting ability and the reactant adsorption capability of the material due to its large surface and multiple scattering effects. These photocatalysts are characterized for the structure, morphology and optical properties by thermogravimetric analysis (TGA), X-ray diffraction (XRD), transmission electron microscopy (TEM), high-resolution

transmission electron microscopy (HRTEM) and UV-vis diffuse reflectance spectra (DRS). Methylene blue (MB) was used as the model substance to evaluate the photocatalytic activity of the photocatalysts. The results indicated that ZnO nanoparticles dispersed uniformly on the mpg-C_3N_4 sheet. The ZnO/mpg-C_3N_4 composite photocatalyst exhibited much higher photocatalytic activity than either pure mpg-C_3N_4 or ZnO, which is due to improvement of separation efficiency of photogenerated electron-hole pairs in ZnO/mpg-C_3N_4 composites.

2. Experimental

2.1 Material

Cyanamide ($CN-NH_2$) was purchased from Rugao City Zhongru Chemical Co., Ltd, P. R. China. 40% dispersion of SiO_2 particleswas supplied by Beijing BOYU GOKE New Material Technology Co., Ltd, P. R. China. The particle diameter of SiO_2 particles is about 12 nm, and the TEM of SiO_2 particles is shown in Figure S1.All other reagents used in this research were analytically pure and used without further purification.

2.2 Sample preparation

2.2.1 Synthesis of mpg-C_3N_4

The mpg-C_3N_4 was synthesized with the hard template method as previously reported[33]. 9.0 g of molten cyanamide was added dropwise in 22.5 g of a 40 % dispersion of 12-nm SiO_2 particles, which were used as a hard template. The mixture was heated at 90 ℃ with stirring to evaporate water. The resultant white powder was then heated at a rate of 2.3 ℃ min^{-1} over 4 h to reach a temperature of 550 ℃, and

then tempered at this temperature for an additional 4 h. The brown-yellow product was treated with ammonium bifluoride (NH_4HF_2, 4 M) for 48 h to remove the silica template. The powders were then centrifuged and washed with distilled water for four times and with ethanol twice. Finally the mpg-C_3N_4 was dried at 70 °C under vacuum for overnight.

2.2.2 Synthesis of ZnO/mpg-C_3N_4 composite photocatalyst

ZnO/mpg-C_3N_4 photocatalysts were obtained via solvothermal method. The preparation processes are showed in Figure 1. Briefly, an appropriate amount of mpg-C_3N_4 was added into 50 mL of ethylene glycol (EG) by ultrasonic treatment for 30 min to completely disperse the mpg-C_3N_4. This was followed by addition of 0.6 g of zinc acetate dissolved in 60 mL of EG and stirring to the obtained a homogeneous dispersion. Subsequently, 219 mg of NaOH which has been dissolved in 50 mL of EG was added to the mixture followed by stirring for 1 h to obtain a homogeneous suspension. The suspension was transferred to a 200 mL Teflon-lined stainless steel autoclave, and maintained at 160 °C for 24 h to achieve the deposition of ZnO on mpg-C_3N_4. Finally, the resultant composite was recovered by centrifugation and washed with absolute ethanol and deionized water five times and dried in an oven at 70 °C for 24 h. A series of ZnO/mpg-C_3N_4 photocatalysts with the different mass ratios of ZnO were prepared by this method, which were denoted as ZnO/mpg-C_3N_4-X, X represented weight percentage of ZnO in ZnO/mpg-C_3N_4 photocatalyst which is determined according to thermogravimetric analysis (TGA)

results. For comparison, ZnO without mpg-C_3N_4 was also obtained by using the same method under the same conditions.

2.3 Characterization

Thermogravimetric analysis was performed in air at a heating rate of 10 °C min^{-1} on a DSC-60 thermal analyzer. The crystallinity of the as-prepared sample was characterized by X-ray diffraction (XRD) on Bruker D8 Advance X-ray diffractometer at room temperature. Morphologies and structures of the prepared samples were further examined with a HITACHI HT770 transmission electron microscopy (TEM) operated at an accelerating voltage of 100 kV and LEO-1530 field emission scanning electron microscope (SEM). High-resolution transmission electron microscopy (HRTEM) images were obtained by a JEOL JEM-2011F field emission transmission electron microscope with an accelerating voltage of 200 kV. The composition of the as-prepared sample was determined by energy-dispersive X-ray (EDX) spectroscopy attached on the same microscope. The UV-vis diffuse reflectance spectras (DRS) of the samples were carried out on a Hitachi U-3010 UV-vis spectrophotometer using $BaSO_4$ as the reference. Fourier transform infrared (FTIR) spectra were carried on a Bruker spectrometer in the frequency range of 2000-600 cm^{-1} with a resolution of 1 cm^{-1}. Raman spectra were recorded on a Horiba HR 800 spectrometer in the range of 400-2000 cm^{-1}. The excitation light was 785 nm. Electrochemical and photoelectrochemical measurements were performed in three-electrode quartz cells with a 0.1 M Na_2SO_4 electrolyte solution. Platinum wire was used as the counter electrode, and saturated calomel electrodes (SCE) were used

as the reference electrodes, respectively. The as-prepared photocatalyst film electrodes on ITO served as the working electrode. The photocurrents were measured on an electrochemical system (CHI-660B, China). Electrochemical impedance spectra (EIS) were measured at 0.0 V. A sinusoidal ac perturbation of 5 mV was applied to the electrode over the frequency range of 0.05-105 Hz. Photoluminescence spectra (PL) of the samples were obtained at room temperature excited by incident light of 375 nm using a fluorescence spectrometer (JASCO FP-6500). Moreover, the concentration of dye and their by-products were determined by HPLC (high performance liquid chromatography) using a Venusil XBP-C_{18} (3.9 × 200, Agela Technologies Inc.) column, Auto-sampler: 20 vials capacity with 6 line degasser channel, K-2501 ultraviolet absorbance detector. Two different kinds of solvents were prepared in this study. Solvent A was acetonitrile while solvent B was made from 0.1 M ammonium acetate and acetic acid (pH 5.3). The flow rate of the mobile phase was set at 0.8 ml/min. Before the analysis, the samples were filtered through Millipore discs of 0.45 μm to protect the chromatographic column.

2.4 **Photodegradation experiment**

The photocatalytic activities were evaluated by the decomposition of methylene blue (MB) under visible light irradiation ($\lambda > 420$ nm) and simulated solar irradiation. The radial flux was measured by a power meter from the Institute of Electric Light Sources, Beijing. Visible irradiation was obtained from a 500 W xenon lamp (Xujiang Electromechanical Plant, Nanjing, China) with a 420 nm cutoff filter. Simulated solar irradiation was provided by a 500 W xenon lamp without the cutoff filter. In each run,

25 mg photocatalyst was totally dispersed in an aqueous solution of MB (50 ml, 0.04 mM). Before irradiation, the suspensions were magnetically stirred in the dark for 120 min to get absorption-desorption equilibrium between the photocatalyst and MB. At certain time intervals, 3 mL aliquots were sampled and centrifuged to remove the particles. The concentration of the MB was analyzed by a Hitachi U-3010 UV-vis spectrophotometer at 663 nm.

3. Results and discussion

3.1 Heterojunction Structure of ZnO/mpg-C_3N_4 photocatalysts

To understand the thermostability of the composites, as well as the ZnO contents in the final products, thermogravimetric analysis was first performed from room temperature to 900 °C at a heating rate of 10 °C min^{-1}. As can be seen in Figure 1, For pure ZnO, a weight loss occurring from 200 °C to 400 °C could be attributed to the desorption of surface bound water. For pure mpg-C_3N_4, two weight loss regions could be seen in the TG curve. The first weight loss from 200 °C to 400 °C could also be attributed to the desorption of surface bound water. The second weight loss occurring from 500 °C to 720 °C could be assigned to the burning of mpg-C_3N_4. For all ZnO/mpg-C_3N_4 samples, these two weight loss regions could also be observed in their TG curves. The amount of ZnO in ZnO/mpg-C_3N_4 composite could be calculated from the second weight loss and is shown in Figure 2. So the really ZnO contents in ZnO/mpg-C_3N_4 composites were determined to be 93.2, 80.3, 65.1, 38.4, 24.9 and 13.8%, respectively.

Figure 3 shows the XRD patterns of the as-prepared ZnO/mpg-C_3N_4 composites, as well as pure mpg-C_3N_4 and ZnO. The mpg-C_3N_4 sample has a characteristic peak at 27.4°, which can be indexed as the (002) diffraction plane. The XRD pattern of pure ZnO has nine discernible diffraction peaks, which confirms the face-centered cubic structure of ZnO according to JCPDS 65-3411. The ZnO/mpg-C_3N_4 composite samples exhibit diffraction peaks corresponding to both mpg-C_3N_4 and ZnO, reflecting the presence of two phases, and no other impurity peaks were observed.

Figure 4 gives the FTIR spectroscopy of ZnO/mpg-C_3N_4 composites. In the FT-IR spectrum of C_3N_4, the peak at 1637 cm^{-1} is attributable to the C=N stretching vibration modes, while the peaks at 1243 cm^{-1}, 1320 cm^{-1} and 1403 cm^{-1} are due to the aromatic C-N stretching[34-36]. The peak at 808 cm^{-1} is related to the s-triazine ring modes[36]. These peaks are all present in the ZnO/mpg-C_3N_4 composites, suggesting that no structural change of g-C_3N_4 occurs during the solvothermal process. Furthermore, with the increase of the mass ratio of the mpg-C_3N_4 to ZnO, the intensities of these characteristic peaks of g-C_3N_4 in the ZnO/mpg-C_3N_4 samples increase.

Raman spectroscopy was carried out to study the structure changes between the pure mpg-C_3N_4 and ZnO/mpg-C_3N_4 composites. Raman spectra of the mpg-C_3N_4 and ZnO/mpg-C_3N_4 samples with the different mass ratio (Figure S2, Supporting Information) all show typical Raman peaks of mpg-C_3N_4, indicating mpg-C_3N_4 in ZnO/mpg-C_3N_4 composites during the solvothermal process retain the same crystal structure of C_3N_4. Furthermore, as increasing the mass ratio of the mpg-C_3N_4 to ZnO,

the intensity of the characteristic peak of C_3N_4 in the ZnO/mpg-C_3N_4 samples increases.

The morphology and microstructure of the representative samples were examined by using SEM, TEM and HTEM. Figure S3 (Supporting Information) gives the SEM micrographs of ZnO, mpg-C_3N_4, and ZnO/mpg-C_3N_4-24.9. The ZnO prepared by the solvothermal method is mainly approximately spherical particles (Figure S3a). The possible reason for the formation of spherical ZnO nanocrystals is that the addition of OH^- caused fast reaction rate, which might cause more nuclei to form in a short time[37]. Figure S3b shows that the image of the mpg-C_3N_4 is composed of a large number of irregular particles. The surface of the mpg-C_3N_4 is fluffy and coarse. Compared with the pure mpg-C_3N_4 phase, the mpg-C_3N_4 in the ZnO/mpg-C_3N_4-24.9 becomes smooth (Figure S3c), suggesting that the fragments of mpg-C_3N_4 can grow into a large sheet structure by the solvothermal treatment. It can also be observed that there are many ZnO particle agglomerations on the surface of mpg-C_3N_4 plates.

Figure 5 shows TEM images of ZnO, mpg-C_3N_4 and ZnO/mpg-C_3N_4-24.9. The pure ZnO are approximately spherical particles with diameters at range of 10~30 nm (Figure 5a). In the image of mpg-C_3N_4 (Figure 5b), many spherical pores with a mean diameter of about 12 nm are observed on the surface of the mpg-C_3N_4. These pores exactly reflect the geometric properties of the original template of SiO_2 particles, which have particle size of 12 nm. Compared with the pure mpg-C_3N_4, the sheet layers of g-C_3N_4 in ZnO/mpg-C_3N_4 composite become bigger and more integral (Figure 5c), which is consistent with the result of SEM. This fact shows that the

fragments of mpg-C_3N_4 can reorganized and grow under the solvothermal condition. Meanwhile, many ZnO nanoparticles are dispersed uniformly on the mpg-C_3N_4 sheet. Figure 5d shows the HRTEM image of ZnO/mpg-C_3N_4-24.9, which gives the direct evidence of the formation of ZnO nanoparticles on the planes and edges of mpg-C_3N_4 sheets. The lattice spacing of planes is 0.281 nm corresponding to the (100) crystal plane of wurtzite ZnO, which is consistent with the spacing values reported in the JCPDS (No. 65-3411). In addition, the corresponding SAED pattern, as shown in the inset of Figure 5d, confirms that the ZnO nanoparticles have the wurtzite structure and also indicates the successful deposition of ZnO nanoparticles on the surface of mpg-C_3N_4.To further confirm the successful preparation of ZnO/mpg-C_3N_4 composite, the composition of this photocatalysis was detected using EDX showed in Figure S4. It can be seen that C, N, Zn and O all exist in this composite. The Cu element comes from the Cu metal supporter.

UV-vis diffuse reflection was carried out to investigate the optical properties of pure mpg-C_3N_4, pure ZnO and ZnO/mpg-C_3N_4 composite samples. As shown in Figure 6, the pure mpg-C_3N_4 exhibits a fundamental absorption edge at 570 nm, corresponding to the band gap of 2.7 eV. The pure ZnO sample has an absorption edge at 400 nm, which can be attributed to the ZnO band gap of 3.18 eV. Meanwhile, at the high ZnO loading amount (93.2 wt.% and 80.3 wt.%), the composite samples show the same absorbance edge with ZnO, and extend the absorbance to the visible region due to the presence of mpg-C_3N_4. When the loading amount of ZnO further decreasing, the absorbance edge shows a gradual red shift, the ZnO/mpg-C_3N_4

255 composite samples show hybrid absorption features of mpg-C_3N_4 and ZnO, which
256 allows for more efficient utilization of the solar spectrum to create photogenerated
257 electrons and holes.

258 **3.2 Photocatalytic activity and photocurrent of ZnO/mpg-C_3N_4 composite**
259 **photocatalysts**

260 The photocatalytic performance was mainly evaluated by degradation of methylene
261 blue (MB), a hazardous dye as well as a common model to test the photodegradation
262 activity. As shown in Figure 7, significant differences in the catalytic behaviors were
263 observed, and the photodegradation process was fit to pseudo-first-order kinetics in
264 which the value of rate constant k is equal to the corresponding slope of the fitting
265 line. Figure S5 (supporting information) gives the photodegradation of MB in
266 presence of composite catalyst with different percentage of ZnO under visible light
267 irradiation. The blank test confirms that MB is only slightly degraded in the absence
268 of catalysis, indicating that the photolysis effects can be ignored. It can be seen that
269 the photocatalytic activity is enhanced gradually with the loading amount of ZnO
270 decreasing under visible light irradiation, and it reaches the maximum when the
271 loading amount up to 24.9 wt.%, further decreasing the loading amount of ZnO, the
272 photocatalytic activity decreases. The k values of ZnO/mpg-C_3N_4 composites with the
273 different ZnO content are showed in Figure 7a. The ZnO/mpg-C_3N_4 sample with 24.9
274 wt.% ZnO had the highest apparent k of 0.182 h^{-1}, which was about 2.3 times as that
275 of pure mpg-C_3N_4 sample (0.080 h^{-1}). Figure 7 b shows the photocatalytic activity of
276 ZnO/mpg-C_3N_4 composites with the different ZnO content under simulated solar

irradiation. The ZnO/mpg-C_3N_4 samples also exhibits gradual enhanced photodegradation activity with the loading amount of ZnO decreasing (Figure 7b). The apparent k of ZnO/mpg-C_3N_4-24.9 (0.303 h^{-1}) is the highest, which is almost 1.9 times better than that of the pure mpg-C_3N_4 (0.161 h^{-1}).

Photocurrent measurements of the pure mpg-C_3N_4 and optimal ZnO/mpg-C_3N_4-24.9 electrodes were also investigated, which are showed in Figure 8. The transient photocurrent responses of a photocatalyst may directly correlate with the recombination efficiency of the photogenerated carriers.[38-40] A generation of photocurrent with good reproducibility for the samples is observed via four on-off cycles. This indicates that the electrode is stable and the photocurrent is quite reversible. ZnO/mpg-C_3N_4-24.9 electrode is about 2.5 times as high as that of the pure mpg-C_3N_4 electrode, which indicates that the separation efficiency of photogenerated electrons and holes is significantly improved in ZnO/mpg-C_3N_4 sample.

Besides activity, the stability of a photocatalyst is important for its application. In order to determine the stability of our composite photocatalysts, 24h persistent MB photodegradation of ZnO/mpg-C_3N_4-24.9 composite was performed, which are showed in Figure 9. The result showed that no obvious loss of photocatalytic activity was observed after irradiation for 24h. Consequently, the ZnO/mpg-C_3N_4 photocatalysts showed good stability during the photocatalytic reaction.

3.3 **Mechanism of degradation and photocatalytic activity enhancement**

To reveal the photocatalytic process, the HPLC chromatograms of the initially MB solution and after different irradiation times of photocatalytic degradation over

optimal ZnO/mpg-C_3N_4-24.9 and pure mpg-C_3N_4 were recorded and shown in Figure 10. It can be seen that two peaks at 4.6 and 4.2 min are detected from the chromatogram spectra of the original reaction solution. The peak at 4.6 min is attributed to the initial MB. Another peak at 4.2 min is attributed to the azure B due to the self-degradation of MB. Under visible light irradiation, two new peaks located at 3.8 and 3.4 min appear, indicating the formation of the intermediate products during the MB photodegradation process. Consequently, photodegradation of the MB solutions not only caused its decoloration but also fractionally destroyed the structure of the MB molecules. According to the literature, the intermediates at 3.8 and 3.4 min are attributed to azure A and azure C, which could be formed through demethylation cleavage of one or two methyl group substituents on the amine groups during photodegradation[41]. The intensity of new peaks increased to the maximum value and then decreased along with the irradiation time, testifying the degradation ability of samples for all the intermediates. The same retention times for the degradation intermediates by pure mpg-C_3N_4 and ZnO/mpg-C_3N_4-24.9 indicated the identical degraded products, so that both them have the same oxidation mechanism for MB degradation under visible light. Furthermore, it can be seen that the MB can be almost completely degraded by ZnO/mpg-C_3N_4-24.9 within 5h under visible light irradiation, showing that ZnO/mpg-C_3N_4-24.9 has a higher visible light photocatalytic activity than pure mpg-C_3N_4.

It is important to detect main oxidative species in the photocatalytic process for elucidating the photocatalytic mechanism. The main oxidative species in

photocatalytic process are detected through the trapping experiments of radicals using t-BuOH as hydroxyl radical scavenger[42] and CH_2O_2 as holes radical scavenger[43], and purging N_2 as $\cdot O^{2-}$ scavenger[44], respectively. As shown in Figure 11a and b, under visible light, the photocatalytic activity of pure mpg-C_3N_4 and ZnO/mpg-C_3N_4 samples decreases slightly by the addition of t-BuOH and purging N_2 gas, while reduced largely with the addition of CH_2O_2, indicating that holes are the main oxidative species for both of pure mpg-C_3N_4 and ZnO/mpg-C_3N_4 samples. In addition, compared with pure mpg-C_3N_4, the straight slope of ZnO/mpg-C_3N_4 samples with same addition of CH_2O_2 declines more obviously, indicating that there may exist more holes in ZnO/mpg-C_3N_4 system. The ESR technique is also used to detect radicals in reaction systems. ESR results are shown in Figure S6. It can be seen there is no ESR signal in the dark, and also under visible light irradiation. This means that there is hardly any hydroxyl radical or $\cdot O^{2-}$ radical for pure mpg-C_3N_4 and ZnO/mpg-C_3N_4-24.9 samples during the photoreaction process. ESR detection further confirmed that holes play the important role on the degradation of MB, and neither hydroxyl radical nor $\cdot O^{2-}$ radical is the main oxidative species for pure mpg-C_3N_4 and ZnO/mpg-C_3N_4 samples, which is consistent with the former trapping experiments. It should be noted that this result is conflict with the some literature where the oxygen super anion and hydroxyl radicals are the main oxidative species of g-C_3N_4, also confirming with the ESR results. However, based our trapping experiments of radicals and ESR results, we confirmed that holes play an important role in our MB degradation. At the same time, some literature also obtained the same result with

343 ours[45-47]. Therefore, the reason for the different oxidative species of g-C_3N_4 might be
344 that the different morphologies of g-C_3N_4, such as, mesoporous g-C_3N_4 or Nanoplates
345 and Nanorods of g-C_3N_4, and different target substrate in the reaction system.

346 To reveal the photocatalytic mechanism further, the interface charge separation
347 efficiency is investigated by the typical electrochemical impedance spectra (presented
348 as Nyquist plots). Figure 12 shows electrochemical impedance spectra (EIS) Nyquist
349 plots of pure mpg-C_3N_4 and ZnO/mpg-C_3N_4-24.9 electrodes before and after visible
350 light irradiation ($\lambda > 420$ nm). The arc radius on the EIS Nyquist plot can reflect the
351 reaction rate on the surface of the electrode. This smaller arc radius implies a more
352 effective separation of photogenerated electron-hole pairs and a higher efficiency of
353 charge immigration across the electrode/electrolyte interface.[48] The arc radii of
354 ZnO/mpg-C_3N_4-24.9 electrode are smaller than that of pure mpg-C_3N_4 electrode,
355 suggesting that ZnO/mpg-C_3N_4 composite structure can make the separation and
356 immigration of photogenerated electron-hole pairs more efficient, which is in good
357 accordance with the result of the photocurrent measurement.

358 Photoluminescence (PL) technique can be also employed to investigate the
359 migration, transfer and recombination processes of photogenerated electron-hole pairs
360 in semiconductors.[49] As shown in Figure 13, pure mpg-C_3N_4 has a strong, wide peak
361 in the PL spectrum, while the PL peak of the ZnO/mpg-C_3N_4-24.9 composite
362 decreases remarkably, indicating the recombination of electrons and holes is hindered
363 greatly. Thus, the faster separation of photogenerated charges contributes to the
364 enhanced photocatalytic activities of ZnO/mpg-C_3N_4 composites.

On the base of the above information, a synergistic mechanism between ZnO and mpg-C_3N_4 for photocatalysis of MB was proposed as illustrated in Figure 14. Under visible light irradiation ($\lambda > 420$ nm), as shown in Figure 12a, ZnO itself can not be excited, the photodegradation of MB can mainly be attributed to the photogenerated hole oxidation and photoreduction process. Compared with the pure mpg-C_3N_4, the ZnO/mpg-C_3N_4 composite can exhibit remarkable enhancement for degrading MB under visible light. Since CB edge potential of mpg-C_3N_4 (-1.12 eV)[50] is more negative than that of ZnO (-0.5 eV)[51], the photoinduced electrons on mpg-C_3N_4 particle surfaces transfer easily to ZnO via the well developed interface. So the excited electron on mpg-C_3N_4 could directly inject into the CB of ZnO, the electron-hole separations are also driven by the internal reassembly rebuilt electric fields in the two semiconductors. This decreases the strength of electron-hole recombination and leads to large numbers of holes on the mpg-C_3N_4 surface, thus promoting the photocatalytic reactions to degradation MB. Figure 12b gives a possible schematic mechanism of the simulated solar activity. ZnO and mpg-C_3N_4 can be all excited, so the photogenerated holes on ZnO could easily transfer to mpg-C_3N_4, since the valence band (VB) position of ZnO is lower than that of C_3N_4, and the excited electron on mpg-C_3N_4 also could directly inject into the CB of ZnO, making charge separation more efficient and reducing the probability of recombination, leading to an enhanced photocatalytic activity of ZnO/mpg-C_3N_4 under the simulated solar irradiation.

4. Conclusion

In summary, the ZnO/mpg-C_3N_4 composite photocatalyst has been successfully synthesized via a facile solvothermal method. The results show the ZnO nanoparticles with the diameters at range of 10~30 nm are dispersed uniformly on the porous mpg-C_3N_4 sheet. This composites photocatalysts showed obviously superior photocatalytic activity and good stability for the photodegradation of MB under the visible light and simulated solar irradiation. The optimal ZnO content with the highest photocatalytic activity is determined to be 24.9 %, which is almost 2.3 times higher than that of individual mpg-C_3N_4 under the visible light, and 1.9 times under the simulated solar irradiation. This enhancement has been demonstrated to be due to the high separation and easy transfer of photogenerated electron-hole pairs at the heterojunction interfaces derived from the match energy level between the ZnO and mpg-C_3N_4. Radical trap experiments holes are the main oxidative species for both of pure mpg-C_3N_4 and ZnO/mpg-C_3N_4 samples.

Acknowledgement

This present work is supported by the National Natural Science Foundations of China (Grant No.21106138), the Fundamental Research Funds for the Central Universities (Grant No. 2011YXL062), National High Technology Research and Development Program of China (2012AA062701), Open fund of National Laboratory of Mineral Materials (Grant No. 09A003).

Reference

1 S.Y. Chai, Y.J. Kim, M.H. Jung, A.K. Chakraborty, D. Jung, W.I. Lee, *J.Catal.*, 2009, **262**, 144-149.

2 A. Fujishima and K. Honda, *Nature*, 1972, **238**, 37-38.

3 P. V. Kamat, *Chem Rev.,* 1993, **93**, 267-300.

4 A. Hagfeldt and M. Graetzel, *Chem Rev.*, 1995, **95**, 49-68

5 M. R. Hoffmann, S. T. Martin, W. Choi and D. W. Bahnemann, *Chem Rev.*, 1995, **95**, 69-96.

6 A. L. Linsebigler, G. Lu and J. T. Yates, *Chem Rev.*, 1995, **95**, 735-758.

7 H. Xie, Y. Li, S. Jin, J. Han and X. Zhao, *J. Phys. Chem. C*, 2010, **114**, 9706-9712.

8 M. Tabata, K. Maeda, T. Ishihara, T. Minegishi, T. Takata and K. Domen, *J. Phys. Chem. C*, 2010, **114**, 11215-11220.

9 F. Dong, L. Wu, Y. Sun, M. Fu, Z. Wu and S. C. Lee, *J. Mate. Chem.*, 2011, **21**, 15171-15174.

10 Q. Xiao and C. Yao, *Mater. Chem. Phys.*, 2011, **130**, 5-9.

11 A. Akyol, H.C. Yatmaz, M. Bayramoglu, *Appl. Catal. B: Environ.*, 2004, **54**, 19-24.

12 S. Chakrabarti, B.K. Dutta, *J. Hazard. Mater.*, 2004, **112**, 269-278.

13 X. Wang, K. Maeda, A. Thomas, K. Takanabe, G. Xin, J. M. Carlsson, K. Domen and M. Antonietti, *Nat. Mater.*, 2009, **8**, 76-80.

14 Y. Wang, X. Wang and M. Antonietti, *Angew. Chem. Int. Ed.*, 2012, **51**, 68-89.

15 Y. Zheng, J. Liu, J. Liang, M. Jaroniec and S. Z. Qiao, *Energy Environ. Sci.*, 2012, **5**, 6717-6731.

16 J. Xu, Y. Wang and Y. Zhu, *Langmuir*, 2013, **29**, 10566-10572.

17 M. Zhang, J. Xu, R. Zong and Y. Zhu, *Appl. Catal. B: Environ.*, 2014, **147**, 229-235.

18 X. Wang, X. Chen, A. Thomas, X. Fu and M. Antonietti, *Adv. Mater.*, 2009, **21**, 1609-1612.

19 G. Liu, P. Niu, C. Sun, S. C. Smith, Z. Chen, G. Q. Lu and H.-M. Cheng, *J. Am. Chem. Soc.*, 2010, **132**, 11642-11648.

20 X.-H. Li, J.-S. Chen, X. Wang, J. Sun and M. Antonietti, *J. Am. Chem. Soc.*, 2011, **133**, 8074-8077.

21 Q. Xiang, J. Yu and M. Jaroniec, *J. Phys. Chem. C*, 2011, **115**, 7355-7363.

22 Y. Sui, J. Liu, Y. Zhang, X. Tian and W. Chen, *Nanoscale*, 2013, **5**, 9150-9155.

23 Y. He, J. Cai, T. Li, Y. Wu, Y. Yi, M. Luo, L. Zhao, *Ind. Eng. Chem. Res.*, 2012, **51**, 14729-14737

24 K. Katsumata, R. Motoyoshi, N. Matsushita, K. Okada, *J. Hazard. Mater.*, 2013, **260**, 475-482.

25 Z. Lin, X. Wang, *Angew. Chem. Int. Ed.*, 2013,**52**, 1735-1738.

26 Y. Cui, Z. Ding, X. Fu, X. Wang, *Angew. Chem. Int. Ed.*, 2012,**51**, 11814-11818

27 J. Zhang, M. Zhang, R.-Q. Sun, X. Wang, *Angew. Chem.,*2012,**124**,10292-10296.

28 J.-X. Sun, Y.-P. Yuan, L.-G. Qiu, X. Jiang, A.-J. Xie, Y.-H. Shen and J.-F. Zhu, *Dalton Trans.,* 2012, **41**, 6756–6763.

29 W. Liu, M. Wang, C. Xu, S. Chen, X. Fu, *J. Mol. Catal. A: Chem.,* 2013,**368–369**, 9-15.

30 W. Liu, M. Wang, C. Xu, S. Chen, *Chem. Eng. J.,* 2012, **209**, 386-393

31 Y. Wang, R. Shi, J. Lin and Y. Zhu, *Energy Environ. Sci.*, 2011, **4**, 2922-2929.

32 D. Chen, K. Wang, D. Xiang, R. Zong, W. Yao and Y. Zhu, *Appl. Catal. B: Environ.*, 2014, **147**, 554-561.

33 F. Goettmann, A. Fischer, M. Antonietti and A. Thomas, *Angew. Chem. Int. Ed.*, 2006, **45**, 4467-4471.

34 Y. C. Zhao, D. L. Yu, H. W. Zhou, Y. J. Tian and O. Yanagisawa, *J. Mater. Sci.*, 2005, **40**, 2645-2647.

35 X. Li, J. Zhang, L. Shen, Y. Ma, W. Lei, Q. Cui and G. Zou, *Appl. Phys. A*, 2009, **94**, 387-392.

36 L. Liu, D. Ma, H. Zheng, X. Li, M. Cheng and X. Bao, *Microporous Mesoporous Mater.*, 2008, **110**, 216-222.

37 A. Famengo, S. Anantharaman, G. Ischia, V. Causin, M. M. Natile, C. Maccato, E. Tondello, H. Bertagnolli and S. Gross, *Eur. J. Inorg. Chem.*, 2009, **2009**, 5017-5028.

38 H. Liu, S. Cheng, M. Wu, H. Wu, J. Zhang, W. Li and C. Cao, *J. Phys. Chem. A*, 2000, **104**, 7016-7020.

39 W. H. Leng, Z. Zhang, J. Q. Zhang and C. N. Cao, *J. Phys. Chem. B*, 2005, **109**, 15008-15023.

40 H. Park and W. Choi, *J. Phys. Chem. B*, 2003, **107**, 3885-3890.

41 M. A. Rauf, M. A. Meetani, A. Khaleel and A. Ahmed, *Chem. Eng. J.*, 2010, **157**, 373-378.

42 H. Lee and W. Choi, *Environ. Sci. Technol.*, 2002, **36**, 3872-3878.

43 T. Tan, D. Beydoun and R. Amal, *J. Photochem. Photobiol. A: Chem.*, 2003, **159**, 273-280.

44 C. Pan and Y. Zhu, *Environ. Sci. Technol.*, 2010, **44**, 5570-5574.

45 X. Bai, R. Zong, C. Li, D. Liu, Y. Liu and Y. Zhu, *Appl. Catal. B: Environ.*, 2014, **147**, 82-91.

46 S. C. Yan, Z. S. Li and Z. G. Zou, *Langmuir*, 2010, **26**, 3894-3901.

47 G. Dong, K. Zhao and L. Zhang, *Chem. Commun.*, 2012,**48**, 6178-6180

48 S. J. Hong, S. Lee, J. S. Jang and J. S. Lee, *Energy Environ. Sci.*, 2011, **4**, 1781-1787.

49 Y.-S. Xu and W.-D. Zhang, *ChemCatChem*, 2013, **5**, 2343-2351.

50 S. C. Yan, S. B. Lv, Z. S. Li and Z. G. Zou, *Dalton Trans.*, 2010, **39**, 1488-1491.

51 H. Fu, T. Xu, S. Zhu and Y. Zhu, *Environ. Sci. Technol.*, 2008, **42**, 8064-8069.

Figure

Figure 1. Preparation of ZnO doped mpg-C_3N_4 photocatalyst via a solvothermal process

Figure 2. TG thermograms for heating the ZnO, mpg-C_3N_4 and ZnO/mpg-C_3N_4 photocatalysts to 900 °C at a heating rate of 10 °C/min

Figure 3. XRD patterns of ZnO, mpg-C_3N_4 and ZnO/mpg-C_3N_4 photocatalysts.

Figure 4. FT-IR spectra of ZnO, mpg-C_3N_4 and ZnO/mpg-C_3N_4 photocatalysts

Figure 5. TEM images of (a) ZnO, (b) mpg-C_3N_4, (c) ZnO/mpg-C_3N_4-24.9, and HTEM image of (d) ZnO/mpg-C_3N_4-24.9, the inset is SAED pattern.

Figure 6. UV-vis diffuse reflection spectra of ZnO, mpg-C_3N_4 and ZnO/mpg-C_3N_4 photocatalysts

Figure 7. Apparent rate constants for the photocatalytic degradation of MB over ZnO, mpg-C_3N_4 and ZnO/mpg-C_3N_4 photocatalysts (a) under visible light irradiation ($\lambda > 420$ nm) and (b) under simulated solar irradiation

Figure 8. The transient photocurrent density responses of pure mpg-C_3N_4 and optimal ZnO/mpg-C_3N_4-24.9 samples electrodes with light on/off cycles under visible light irradiation ($\lambda > 420$ nm) [Na_2SO_4] = 0.1 M

Figure 9. Photostability experiments in the presence of ZnO/mpg-C_3N_4-24.9 composite under visible light irradiation ($\lambda > 420$ nm)

Figure 10. HPLC Chromatogram of MB photodegradation by pure mpg-C_3N_4 and optimal ZnO/mpg-C_3N_4-24.9 under visible light irradiation ($\lambda > 420$ nm)

Figure 11. The plots of photogenerated carriers trapping in the system of photodegradation of MB by (a) pure mpg-C_3N_4 and (b) ZnO/mpg-C_3N_4-24.9, under visible light irradiation ($\lambda > 420$ nm), respectively

Figure 12. Nyquist plots for pure mpg-C_3N_4 and ZnO/mpg-C_3N_4-24.9 in aqueous solution in the dark and under visible light illumination ($\lambda > 420$ nm) [Na_2SO_4 = 0.1 M]

Figure 13. Photoluminescence spectra of mpg-C_3N_4 and ZnO/mpg-C_3N_4 photocatalysts

Figure 14. Schematic drawing illustrating the mechanism of charge separation and photocatalytic activity of the ZnO/mpg-C_3N_4 photocatalyst (a) under visible light irradiation ($\lambda > 420$ nm) and (b) under simulated solar irradiation

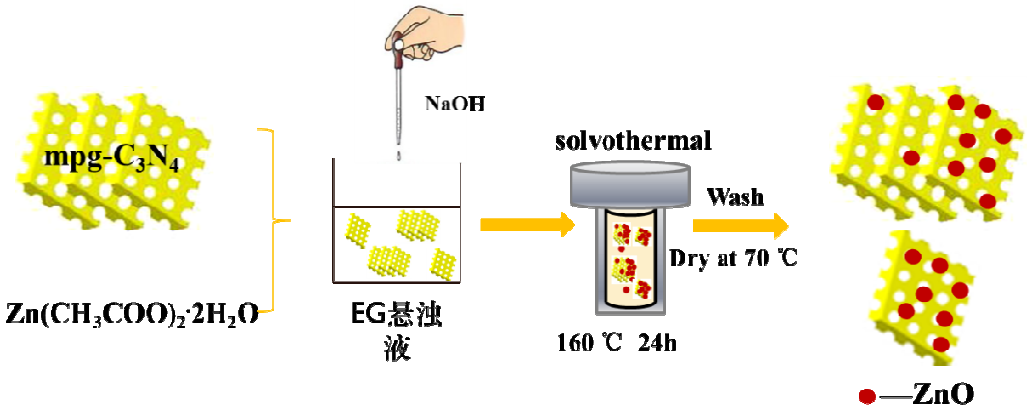

Figure 1

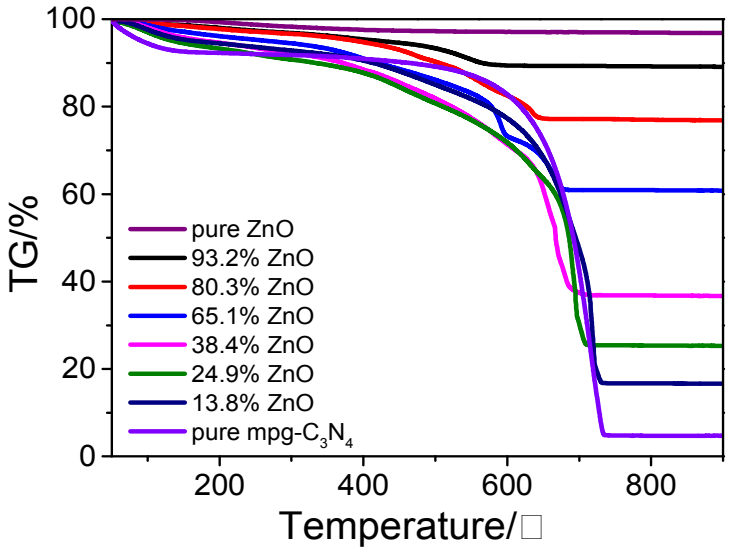

Figure 2

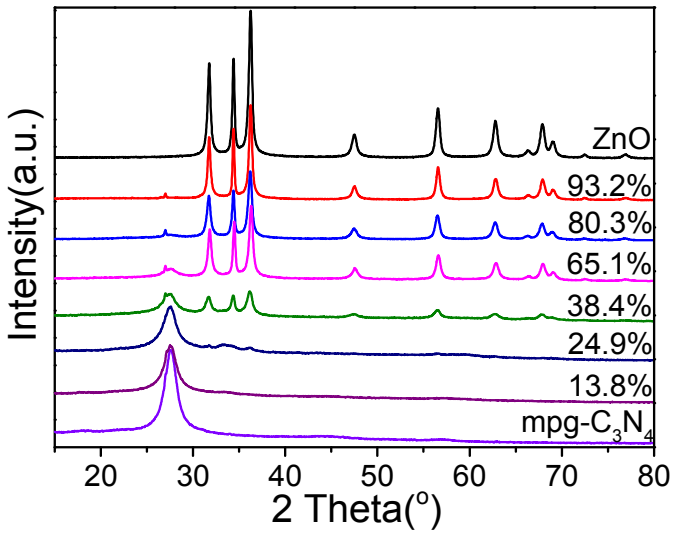

Figure 3

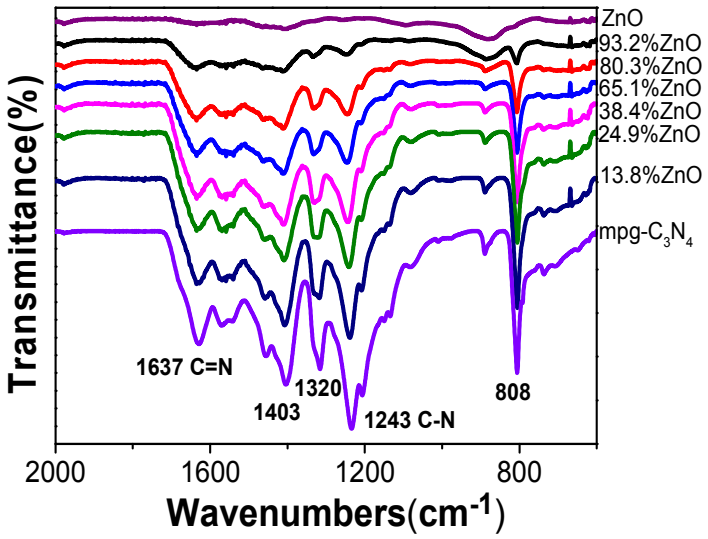

Figure 4

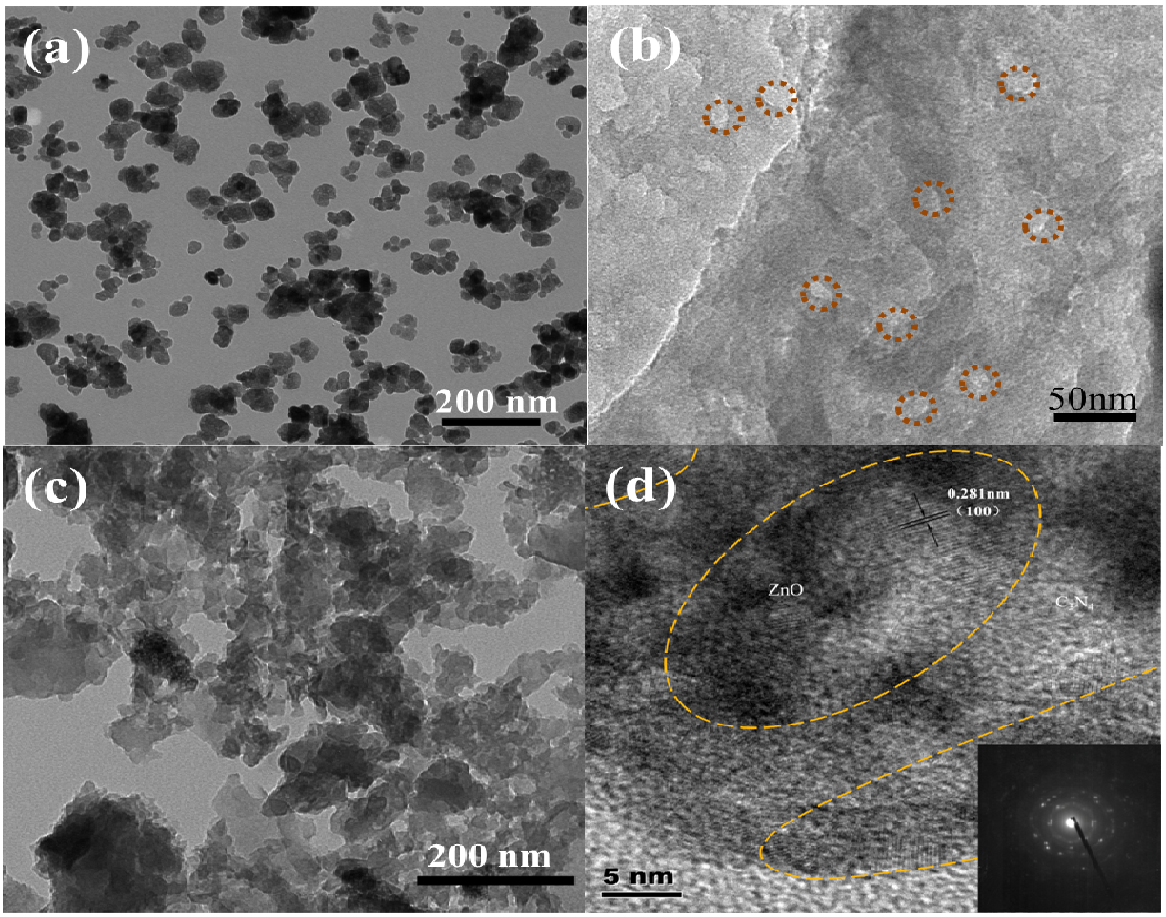

Figure 5

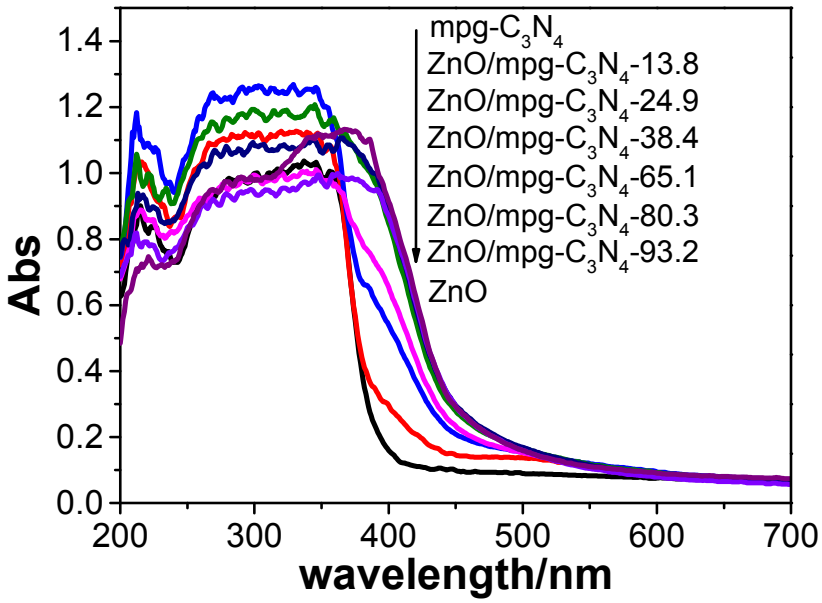

Figure 6

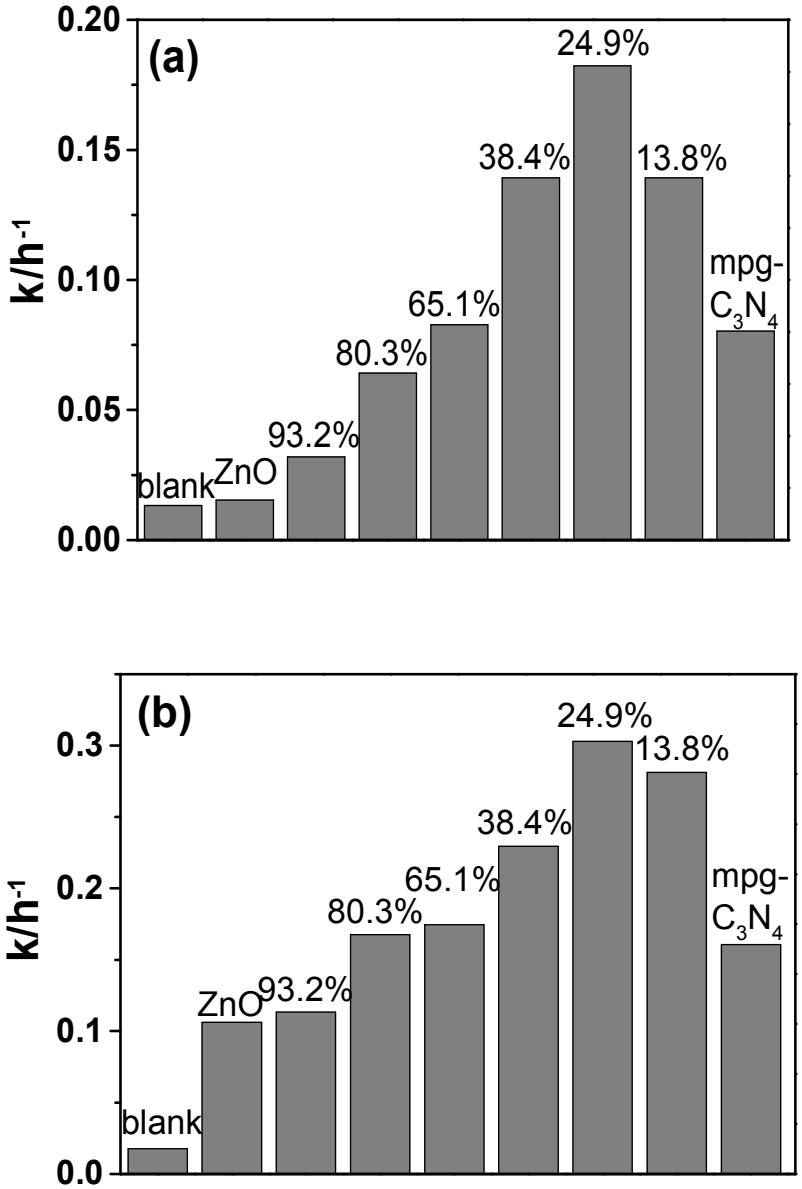

Figure 7

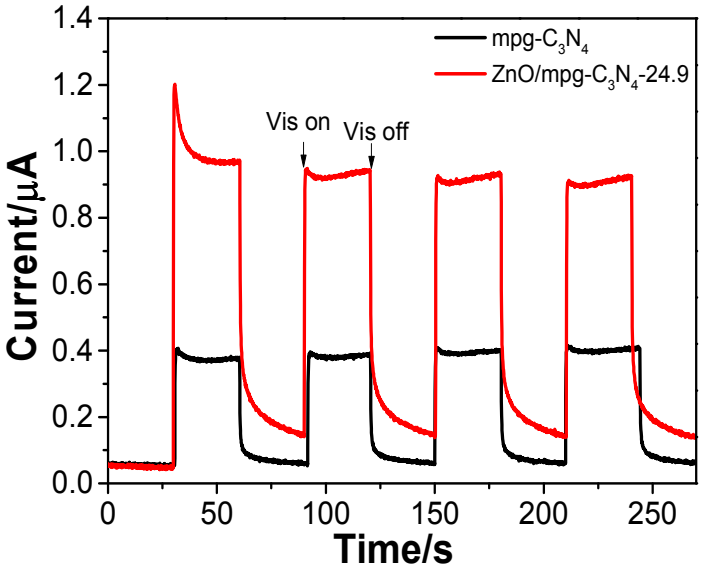

Figure 8

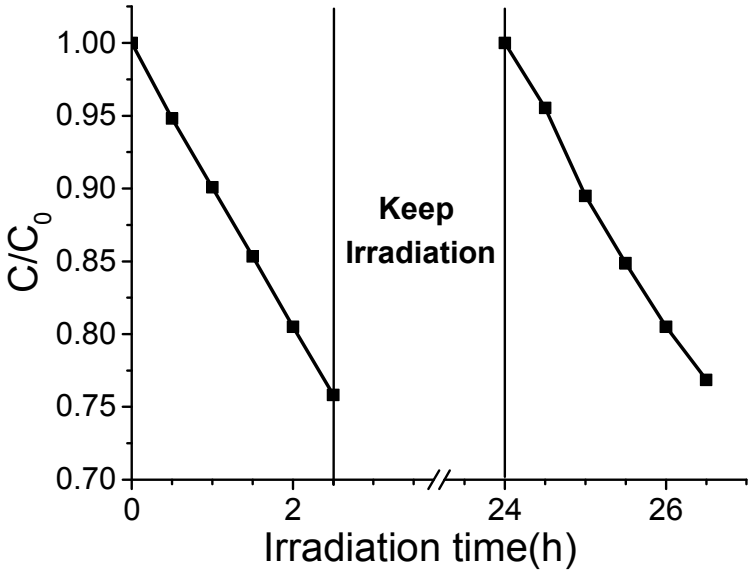

Figure 9

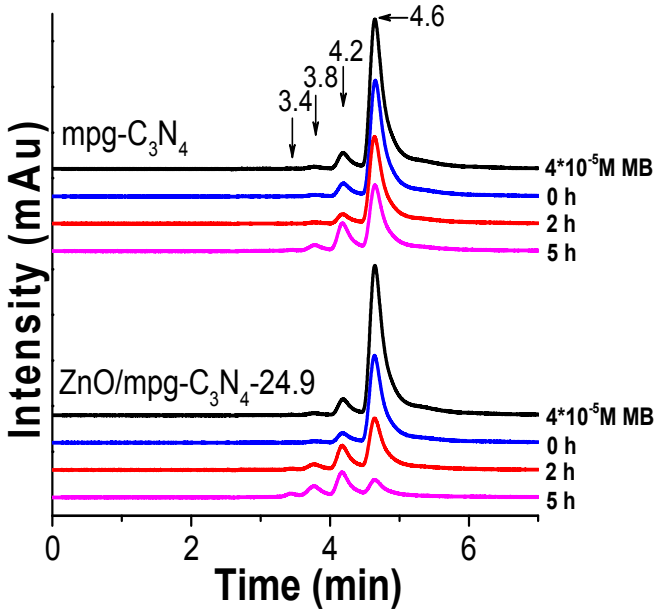

Figure 10

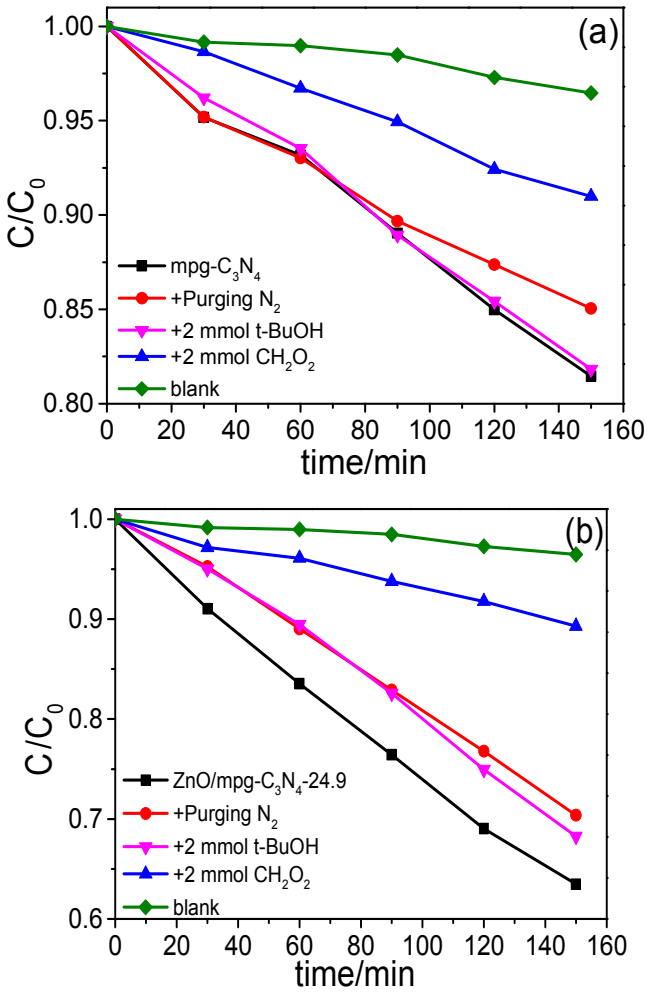

Figure 11

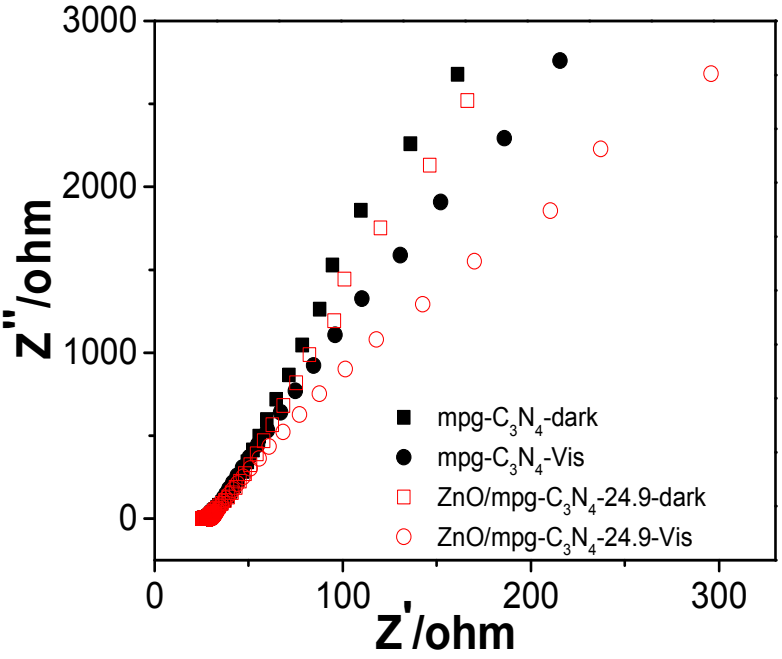

Figure 12

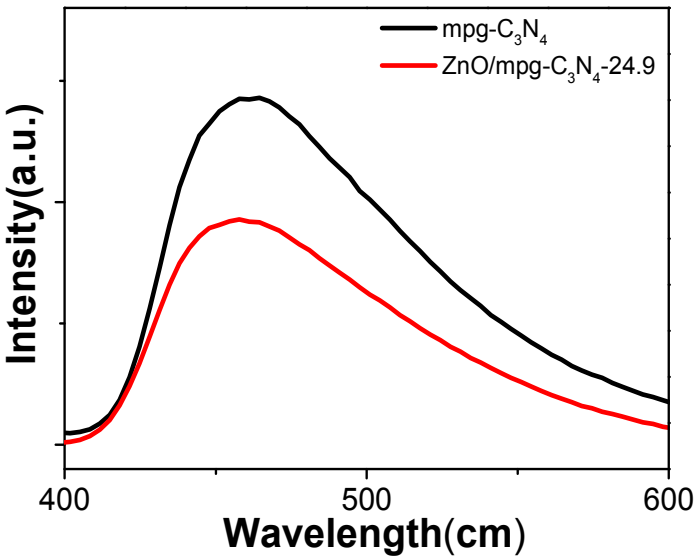

Figure 13

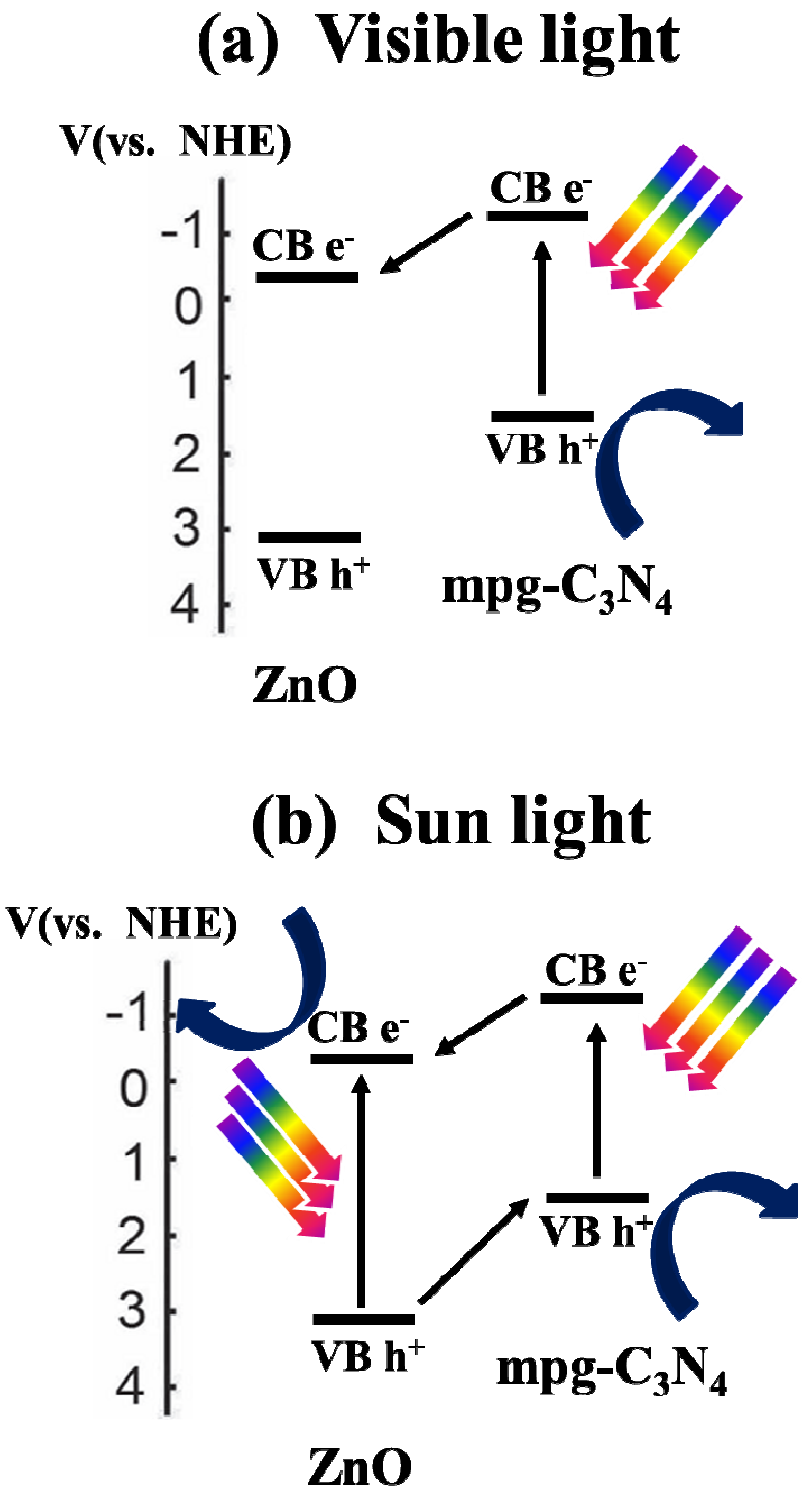

Figure 14

Graphical abstract

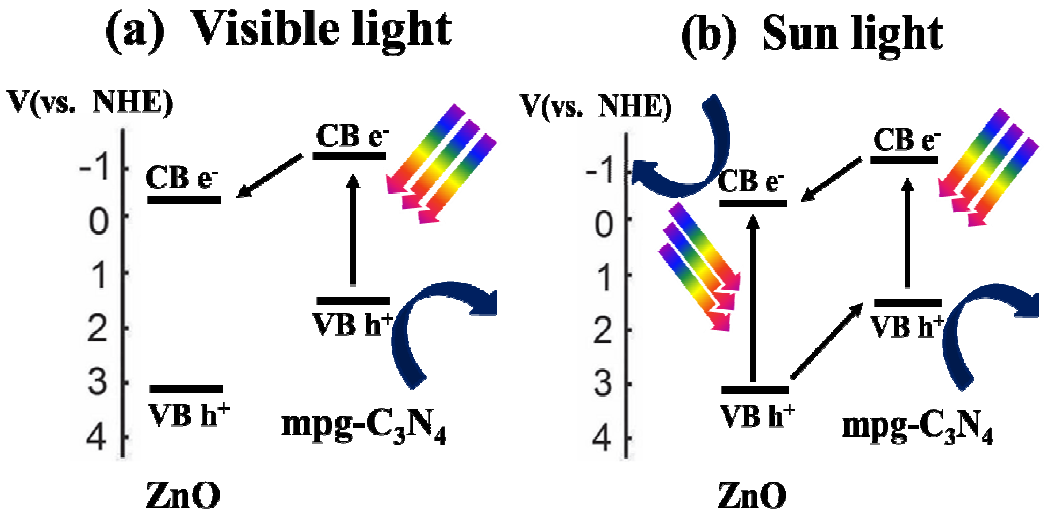

The photocatalytic activity enhancement of the ZnO/mpg-C_3N_4 is due to the high separation and easy transfer of photogenerated electron-hole pairs.